An Effective Growth of Hierarchical BNNTs/SiC Fibers with Enhanced Interfacial Properties

Deniz Köken[A], *Ayşemin Top*[D], *Fevzi Çakmak Cebeci*[A, B ‡], *Fırat Turgut*[D], *Beyza Bozali*[D], *Elif Özden-Yenigün*[E], *Nuri Solak*[F], *Hülya Cebeci*[C, D, *]

[A]Faculty of Engineering and Natural Science, Sabancı University, 34956, Turkey
[B]SUNUM Nanotechnology Research Center, Sabancı University, 34956, Turkey
[C]Faculty of Aeronautics and Astronautics, Istanbul Technical University, 34467, Turkey
[D]Aerospace Research Center, Istanbul Technical University, 34467, Turkey
[E]School of Design, Textiles, Royal College of Art, SW7 2EU, United Kingdom
[F]Faculty of Chemical and Metallurgical Engineering, Istanbul Technical University, 34467, Turkey
[‡] Corresponding author at: Faculty of Engineering and Natural Science, Sabancı University, 34956, Turkey. Tel.: +902164839877
E-mail address: fccebeci@sabanciuniv.edu
[*]Corresponding author at: Faculty of Aeronautics and Astronautics, Istanbul Technical University, 34467, Turkey. Tel.: +902122853134
E-mail address: hulya.cebeci@itu.edu.tr

Tailoring the SiC fiber-matrix interface in micron-sized fibers is crucial to attaining enhanced mechanical properties in ceramic reinforced composites. Herein, the authors report the growth of boron nitride nanotubes (BNNT) onto SiC fibers (SiC_f), creating a fuzzy fiber architecture to promote the surface area for a defined load path fiber to the matrix and improve the mechanical properties of these structures. Successful BNNT-growth is achieved by a boron oxide chemical vapor deposition method combined with growth vapor trapping with optimum parameters of 1200 °C and 1 hour, comparatively low temperature to those reported in the literature. The strength loss of SiC_f after exposure to 1200 °C was attributed to high process temperature, similar to what has been observed in the literature. Hence, BNNT growth does not lead to additional strength loss on these fibers measured by a single fiber tensile test. Moreover, through this direct growth method, grown BNNTs utilize a surface-anchored BNNTs/SiC_f, creating a good matrix adhesion to prevent fiber-fiber sliding and pullout and increasing the interfacial shear strength (IFSS) with epoxy. Furthermore, microbond tests show that fuzzy BNNTs/SiC_f architecture increased IFSS by at least 87.8% compared to as-received SiC_f.

Keywords: A. Nano-structures, A. Ceramic fibers, B. Interface/interphase, D. Mechanical Testing.

1. Introduction

Ceramic matrix composites (CMCs) composed of SiC fibers (SiC_f) and a SiC matrix (SiC_f/SiC) are lightweight thermostructural composites used in hot sections of gas turbine engines for turbomachinery applications. The mechanical properties of these CMCs are highly influenced by the fiber/matrix (F/M) interface, dominating, in particular, the desired fiber pullout during fracture that will lead to an enhanced fracture toughness through energy dissipation [1]. Hence, a deep understanding and optimization of the F/M interface can bring reliable performances to CMCs for many advanced applications, from commercial aircraft to deep space missions.

F/M interface interactions that are too strong or too weak result in catastrophic failure or low mechanical properties, respectively. The commonly encountered toughness problem in SiC_f/SiC composites arising from F/M interface interaction can be resolved through an interphase design for improved load transfer capability [2]. Among the widely known approaches, coating the SiC_f with a thin film using pyrolytic carbon (PyC) [3], zirconia [4], h-BN, [3, 5, 6] and growing nanotubes onto the surface of the fibers bring numerous advantages in a controlled fashion [7, 8]. Fibers with architectural nanostructures grown in situ, such as nanotubes (NTs), also referred to as “fuzzy fibers”, have a higher surface area than neat fibers and enhance the toughness of the composite by reinforcing the resin-rich regions. This reinforcement also improves stress transfer, resulting in increased interfacial shear strength (IFSS). Additionally, fuzzy fibers may overcome stress concentration at the F/M interface and reform crack formation and propagation.

Lately, an area of particular focus has been on growing carbon nanotubes (CNTs) onto the surface of micron-sized fibers with the potential to expand the performance and functionality of fiber-reinforced composites. To date, Garcia *et al.* [7] have synthesized aligned CNTs onto the surface of alumina fibers in fuzzy form and infused epoxy matrix on the fibers via a simple

layup procedure. Their architecture showed a 69% increase in the interlaminar shear strength (ILSS) in addition to better electrical conductivity. Wicks *et al.* [9] also studied the effect of fuzzy fiber CNTs on the fiber-reinforced polymer matrix finding that the fracture toughness of the composite was enhanced by 76%, as well as achieving a minor increase in critical strength and ultimate strength in tension-bearing tests – 9% and 5% respectively. Additionally, CNTs have been utilized as reinforcements in SiC_f/SiC composites to increase fracture toughness and flexural properties, [10] as an interphase material, [10-14] to achieve electromagnetic shielding [15], and to enhance thermal conductivity [16]. However, all of these mechanical properties and thermal conductivity were noticeably improved by CNTs, the thermo-oxidative stability of CNTs was insufficient, making them unsuitable for high-temperature applications due to their low thermal stability (approximately 400 °C – 600 °C) in the air [17]. To satisfy the high thermal stability requirement in CMCs, Hart *et al.* [8] suggested the growth of Velcro-inspired SiC nanowire and nanotube coating with "fuzzy fiber" architecture. They grew SiC nanostructures on the surface of SiC_f by using CNTs as a template and enhanced Young's modulus of the composite by 47%, with increasing thermal resistance under an oxygen atmosphere. However, the growth of SiC nanostructures on the surface of the SiC_f requires a two-step chemical vapor deposition (CVD) process, starting from growing CNTs and then their conversion to SiC tubes. Furthermore, boron nitride nanotubes (BNNTs) satisfy the requirements of CMCs in a similar fashion to CNTs in the F/M interface through a high specific surface area and very high thermal stability, high corrosion resistance, and excellent mechanical properties at elevated temperatures [18-20]. Hurst *et al.* [21] showed that it is possible to decorate fiber surfaces with BNNTs, and achieved a 2.5 – 3 times higher tensile strength for the BNNTs/SiC_f composite coupons prepared by the thermal CVD method; however, they did not evaluate their interlaminar shear strength (ILSS), which is crucial for such a hybrid approach. Similarly, Zhu *et al.* [22] prepared SiC_f/BNNTs-SiC architectures by growing BNNTs onto SiC_f in-situ via ball milling, and while 87.8% of the SiC_f/SiC strength was retained at elevated temperature,

SiC_f/BNNTs-SiC composites showed 94.7% strength retention. Moreover, no decrease in fracture toughness was reported. Also, there have been studies where BNNTs were used as interface materials in metal matrix composites (MMCs). Nautiyal *et al.* [23] fabricated layered Al-BNNT-Al MMCs using ultra-long BNNTs in which they showed a 400% tensile strength increase compared to neat Al. The results were attributed to an effective load transfer of directionally aligned BNNTs and strong interfacial interaction between the Al matrix and BNNTs. Applying these fuzzy architectures as BNNTs/SiC_f may be used in next-generation CMCs for advanced applications with an industrially compatible approach similar to BN coatings applied onto SiC_f to prevent oxidative environments.

Above mentioned coatings are primarily designed to introduce a weak interface between the fibers and matrix to enhance the toughness of the SiC/SiC composites. Lately, a different approach has started to gain interest [24-27]. Strong interface interactions allow cracks to be arrested within the coating into short and branched cracks. These multicracks increase the toughness of the composites via increased crack density since more cracks can absorb more energy resulting in higher toughness for the composite. Furthermore, improved load transfer leads to enhanced strength for the composite [24]. Overall, the composites' strength, toughness, lifetime, and creep resistance can be enhanced by introducing strong interfaces [26]. Rebillat *et al.* [24] showed that the load necessary to initiate fiber pullout is 4 times higher for the strong interface interaction fibers, and interfacial shear strength is 10 times higher than weak interface SiC/SiC composites. Their results showed that strongly bonded interfaces show more robust mechanical properties and are expected to have a higher fatigue lifetime than weakly bonded counterparts. Pasquier *et al.* [28] also argued the same points discussed by the Rebillat *et al.* and reported that when the strongly bonded interfaces are present, fatigue lifetime and behavior significantly improves for the SiC composites even in elevated temperatures in an oxidizing environment.

The present study explores the F/M interface interactions where BNNTs were grown onto SiC_f, depicted as BNNTs/SiC_f fuzzy fiber architecture. The growth process is performed onto a magnesium/iron catalyst decorated SiC_f via single-step growth vapor-trapping boron oxide chemical vapor deposition (GVT-BOCVD) at 1200 °C, which is lower than reported in the literature [29]. BNNTs were synthesized using elemental boron with a combination of MgO and Fe_2O_3 catalysts as the boron oxide precursor and ammonia as the nitrogen source. The growth temperature and time were studied to reveal the effect on BNNT morphology, and growth yield was optimized through the catalyzing process in detail. We highlighted the preservation of the critical mechanical properties of the SiC_f with BNNT fuzzy architecture forming via a single fiber tensile test. A single fiber microbond study using an epoxy matrix microdroplet test was performed to calculate IFSS that allows comparative data acquiring in a straightforward and easily replicable fashion to understand the contribution of directly synthesized "fuzzy fiber" BNNTs onto fibers, mentioned as "Velcro-like" interactions. The results yielded an 87.8% enhancement in IFSS, with a high yield circumferential BNNT growth onto SiC_f. Although IFSS results were presented through a microbond test using an epoxy matrix, the results are highly promising for further studies that can be translated to CMCs systems.

2. Experimental

2.1. Catalyst coating onto SiC_f

Hi Nicalon S type SiC_f as a tow, with 500 single fibers having a diameter of 17 µm, was received from the Safran Herakles company. The polymer sizing was removed via a chemical de-sizing process involving washing it with Dimethylformamide (DMF) (20 mL) for 48 hours, then drying it off in a vacuum oven overnight at 80 °C. Before catalyst coating, the surface of SiC_f was activated with the oxygen plasma treatment (Harric Plasma, PDS-002 (230V)) for three minutes to achieve a clean and negatively charged surface. Subsequently, SiC_fs with an activated surface were soaked in 2.5 wt. % iron (III)

acetylacetonate (Fe(III)Acc), 2.5 wt. % magnesium acetylacetonate (Mg(Acc)) and an ethanol solution for 15 minutes. The fibers were then dried off in a vacuum oven at 60 °C for an hour to achieve favorable nucleation sites for BNNT growth. Catalyst-coated fibers were first annealed in a furnace at 250 °C under air for an hour to remove any solvent residues. Following the annealing, the catalyst coating was reduced under a hydrogen atmosphere at 500 °C for four hours. This process allowed both Fe^{3+} and Mg^{2+} ions to be reduced to Fe and Mg.

2.2. Growth of "Fuzzy fiber" BNNTs onto SiC_f

The GVT-BOCVD method was performed for the growth of "fuzzy fibers" BNNTs onto SiC_f surfaces. This method is commonly utilized for BNNT growth [30], resulting in high yield at low temperatures compared to other methods using over 1400 °C [29]. Briefly, boron (B) nanopowder was used as a boron precursor mixed with magnesium oxide (MgO) and iron (III) oxide (Fe_2O_3) nanopowder, with a weight ratio of 2:1:1 ($B:MgO:Fe_2O_3$). The alumina boat was covered with silicon wafers to increase the partial pressure of growth vapors inside the reaction zone, enhancing the nucleation probability ($\underline{PN}$) of the BNNTs as depicted in the whisker theory nucleation (Equation 1). $\underline{PN}$ indicates the nucleation probability, B is the constant, σ is the surface energy of the whisker grown, k is the Boltzmann constant, α is supersaturation ratio that corresponds to $\underline{p/p^0}$, (the partial pressure of growth vapors and the partial pressure of the condensed phase at the equilibrium are $\underline{p}$ and $\underline{p^0}$, respectively) and $\underline{T}$ is temperature.

$$PN = B \exp\left(-\frac{\pi\sigma^2}{k^2T^2 \ln \alpha}\right) \quad (1)$$

The alumina boat was then positioned in the sweet spot of the horizontal tube furnace (Protherm PFT 15/50/450). The growth was successfully achieved at optimized 1200 °C in an argon/ammonia atmosphere.

2.3. Characterization

The morphology of as-received SiC_f and BNNTs/SiC_f were investigated by Scanning Electron Microscopy (SEM) (A FEI-Qanta FEG250, USA) and Ultra High-Resolution Transmission Electron Microscopy (Jeolden JEM-200CFEG UHR-TEM CS corrected equipped with Garanti Quantum GIF). Structural characterization of BNNTs was attained using RAMAN spectroscopy (Renishaw inVia Reflex Raman Microscopy and Spectrometer (532 nm laser unit)). The average diameter of the nanotubes was determined by measuring the diameters of 100 different BNNTs on the SEM images of each sample using ImageJ software. X-Ray Diffraction (XRD) (A Bruker TM D8, Cu Kα, 1.542 °A) was performed to understand the crystal structure of SiC_f and BNNTs.

2.4. Sample Preparation for Single Fiber Tensile Test

The tensile strength of as-received SiC_f and BNNT/SiC_f was evaluated via a single fiber tensile test using a Universal Tensile Machine (UTM) (Shimadzu), equipped with 1kN load cell (1mN sensitivity) (**Error! Reference source not found.**(a)). A fiber was first mounted on a paperboard frame with gauge lengths of 25 mm, and the specimen ends were attached to the paperboard using a quick-drying adhesive. Specimens were tested under quasi-static tensile loading at a 0.5 mm/min deformation rate, as defined at ASTM D3379 [31].

The distribution function of strength ($\underline{\sigma}$) as $\underline{P_f}$ was determined by the following Weibull distribution function in Equation 2, where m and σ_0 are the shape and scale parameters, respectively.

$$P_f = 1 - \exp\left[-\left(\frac{\sigma}{\sigma_0}\right)^m\right] \quad (2)$$

In this study, shape and scale parameters were expressed through the linear regression method [32] by sorting the maximum breaking strength of each fiber into ascending order and calculating the failure probability of each fiber using a median rank estimator [33]. Equation 2 can be rearranged as shown in Equation 3 for achieving $\underline{\sigma}$ and $\underline{\sigma_0}$.

$$\mathrm{In}(\mathrm{In}\,\frac{1}{1-\mathrm{P_f}}) = \mathrm{m}.\,\mathrm{In}\sigma - \mathrm{m}.\,\mathrm{In}(\sigma_0)\ [34] \quad (3)$$

2.5. Sample Preparation for Single Fiber Microbond Test

A single fiber microbonding test was performed on as-received SiC_f and BNNT/SiC_f using epoxy microdroplets to identify the IFSS. A fixture was designed and integrated with a UTM to perform the IFSS tests. Epoxy was prepared with the L160 - H160 epoxy resin system from Hexion, and the mixing ratio of resin to hardener was selected as 4:1. Epoxy microdroplets were formed with a hand-held syringe onto the surface of the single fibers, which were aligned on a base plate. Epoxy microdroplets on the fibers were kept at an ambient temperature to be cured for 24 hours.

The IFSS was calculated with Equation 4, and the embedded fiber length ($\underline{l_e}$), fiber diameter ($\underline{d_f}$), and the microdroplet length were measured using an optical microscope, respectively, and $\underline{F_{max}}$ is the maximum load. Results were represented either as the average value of calculated IFSS' or as the slope of the regression line intercepting origin over the force–embedded area plot. Since the measured forces were considerably lower than load cell capacity, the maximum loads obtained from UTM were corrected according to a calibration process explained in detail in supporting information.

$$\tau_{\mathrm{IFSS}} = \frac{\mathrm{F_{max}}}{\pi \mathrm{d_f l_e}} \quad (4)$$

3. Results and Discussion

3.1. Growth of BNNTs

Adjusting the CVD process parameters for tuning the microstructure and morphology of BNNT growth onto SiC_f is crucial to achieving an effective fuzzy fiber hierarchical formation. Hence, to evaluate the effect of growth temperature on the BNNT properties, the morphologies of three different growth temperatures (1200 °C, 1100 °C, and 1000 °C) with the same 60 minutes growth time in the GVT-BOCVD system on SiC_f were revealed by imaging through SEM (Figure 1). The growth results at 1000 °C (**Error! Reference source**

not found.(a)) displayed nucleation sites with no BNNT growth on the fiber's surface, suggesting an insufficient growth temperature. However, synthesis at 1100 °C yielded a successful BNNT coating, with a uniform conformal coverage over the surface of the SiC_f, having smooth morphologies (**Error! Reference source not found.**(b)). Increasing the growth temperature to 1200 °C (**Error! Reference source not found.**(c)) created additional nucleation sites to grow denser BNNT coatings with conformal coverage. Additionally, the SEM images of BNNTs grown at 1100 °C and 1200 °C presented morphologies with similar fashion, and both have close diameter distribution and homogeneity. Moreover, at higher BNNT growth temperatures, the diameter of as-grown BNNTs was increased, and 1200°C was attributed as an optimum synthesis temperature . Hence, after achieving denser and conformally covered BNNTs over the SiC fiber at 1200°C, the growth temperature was not increased further [35].

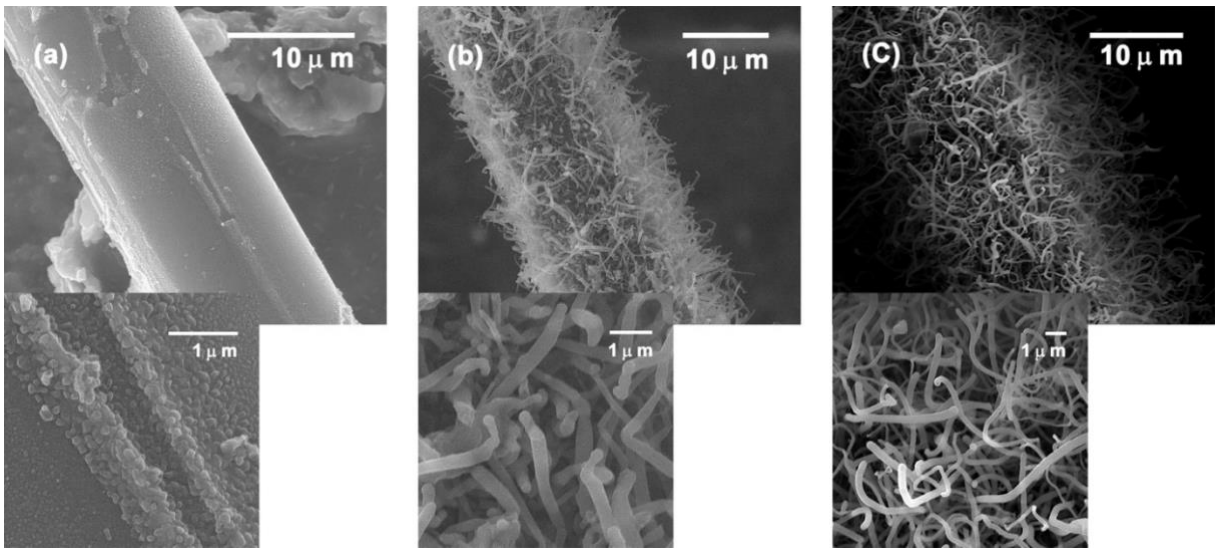

Figure 1. SEM images of different BNNTs grown for 60 minutes at different temperatures. (a) 1000 °C, (b) 1100 °C, (c) 1200 °C.

Since the literature studies report about the poor wettability characteristics of BNNTs [36, 37], overcoming such a challenge is studied by applying plasma treatment onto SiC_f through introducing defects and enhancing the wettability, which is crucial for improved F/M

interface. The SEM images in **Error! Reference source not found.**(a) depicted a baseline of the morphology of desized and plasma-treated as-received SiC_f having a smooth, clean surface with no micro-defects such as pits. The plasma treatment was performed for all SiC_f before catalyst deposition through a dip-coating process. Densely packed BNNTs with a bamboo-like tube morphology and with a diameter range of 80-150 nm were grown onto the SiC_f surface in a randomly oriented fashion in micrometer lengths. These morphologies were referred to as "fuzzy fiber" BNNT architectures, as shown in **Error! Reference source not found.**(b), with a 15 minutes catalyst soaking time described in section 2. Nucleation sites originated from the catalyst particles under the growth conditions employed in nanotube growth can be observed with a uniform distribution onto the selectively etched surface of the fiber, as depicted in **Error! Reference source not found.**(c).

A cross-section image of the BNNT/SiC_f fuzzy morphology, presented in **Error! Reference source not found.**(d), clearly confirmed the preservation of the circular cross-section of the SiC_f after the GVT-BOCVD process at 1200 °C. A uniform and homogeneous catalyst decoration enables strong nanotube-fiber adhesion, and **Error! Reference source not found.**(c) and **Error! Reference source not found.**(d) proved that interlocked curly BNNTs were grown on the surface rather than deposited onto the surface. However, some cone-shaped BNNTs can be attributed to the incomplete growth of tubes due to placing the fibers in between silicon wafer holders for the GVT-BOCVD process. Full coverage of BNNTs along with the fiber with a high surface area and aspect ratio may offer superior F/M interface interactions through BNNTs that are better intertwined with the matrix with hook and loop "Velcro effect" mechanisms [8].

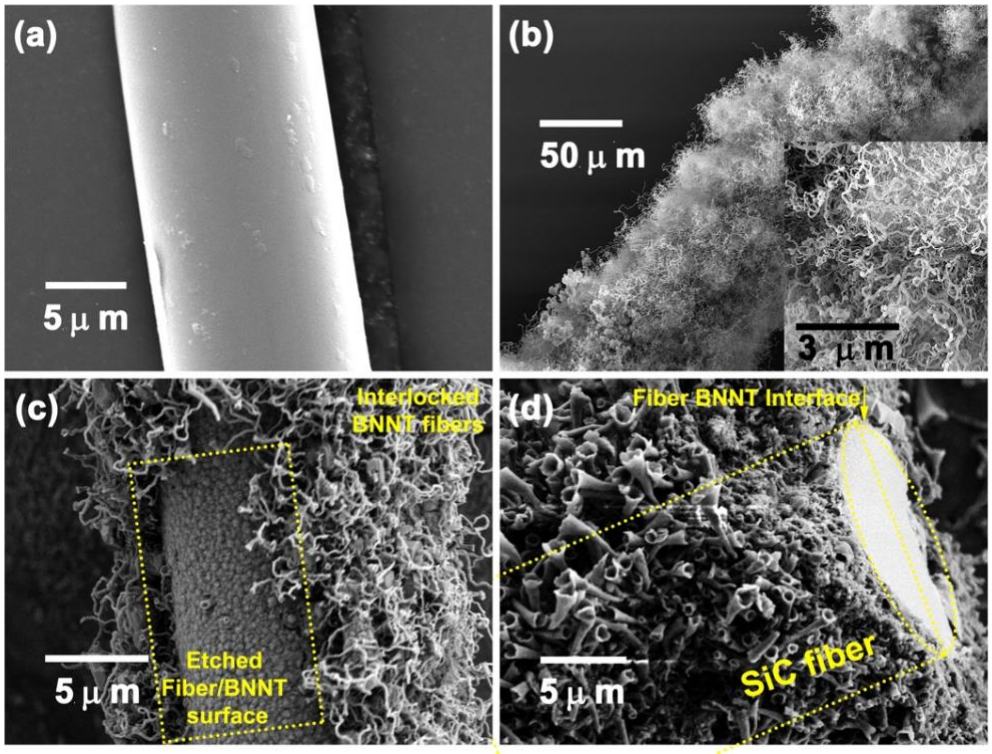

Figure 2. SEM images of (a) chemically desized and then plasma treated SiC_f, (b) SiC_f/BNNTs surface, (c) selectively etched BNNTs/SiC fiber surface, (d) cross-section image of the SiC_f/BNNTs

TEM characterization was performed to gather information about the structure and chemical composition of as-synthesized BNNTs. An HRTEM image showed hollow tube morphology for as-synthesized BNNTs with a ~20 nm diameter (**Error! Reference source not found.**(a)). Dark fringes on the edge of the nanotubes highlighted the multi-walled nanotube structure of the BNNTs. Moreover, the parallel orientation of the walls with respect to the tube axes suggested a zig-zag nanotube structure [38]. Profile analysis from the HRTEM image of a single BNNT was performed to calculate the number of walls (**Error! Reference source not found.**(b)). Each peak on the graphic represented a wall, giving an average number of 30 walls for the as-synthesized BNNTs. The distance between the walls was found to be 0.33 nm, which is consistent with the d_{002} lattice spacing of bulk h-BN [39]. An electron energy loss spectroscopy (EELS) analysis was performed to analyze the chemical composition of the nanotubes. The EELS results (**Error! Reference source not found.**(c))

showed strong B k-edges together with strong N k-edges. Additionally, sp^2-hybridization of h-BN was also clear due to intense π* peaks of B and N, similar to previously reported studies [40].

As-synthesized BNNTs were analyzed by RAMAN and FTIR spectroscopy to provide structural information (**Error! Reference source not found.**(d-e)) and purity. The RAMAN spectra (**Error! Reference source not found.**(e)) showed an intense peak at 1367 cm^{-1} corresponding to the well-defined E_{2g} in-plane vibrational mode of h-BN, and a single, narrow, and intense peak also confirmed the high purity of the BNNTs. Two characteristic absorption bands observed at FTIR analysis (**Error! Reference source not found.**(d)) at ~1348 cm^{-1} and ~1530 cm^{-1} correspond to the plane stretching mode of BNNTs, and an absorption band at ~786 cm^{-1} coincides with the out-of-plane radial buckling mode (R) of BNNTs, which is consistent with the literature [41].

The effect of catalyst decoration on the BNNT growth yield can be deduced distinctly from the SEM images, which belong to the BNNTs/SiC_f with and without catalyst deposition (Figure 2(b), **Error! Reference source not found.**(f)). BNNTs' growth onto the fibers without surface decoration resulted in a low yield and dominant metastable BN phases rather than the desired nanotube structure (**Error! Reference source not found.**(f)). However, the decoration of the surface with the catalyst increased the surface coverage of BNNTs and promoted a successful tube formation (**Error! Reference source not found.**(b)).

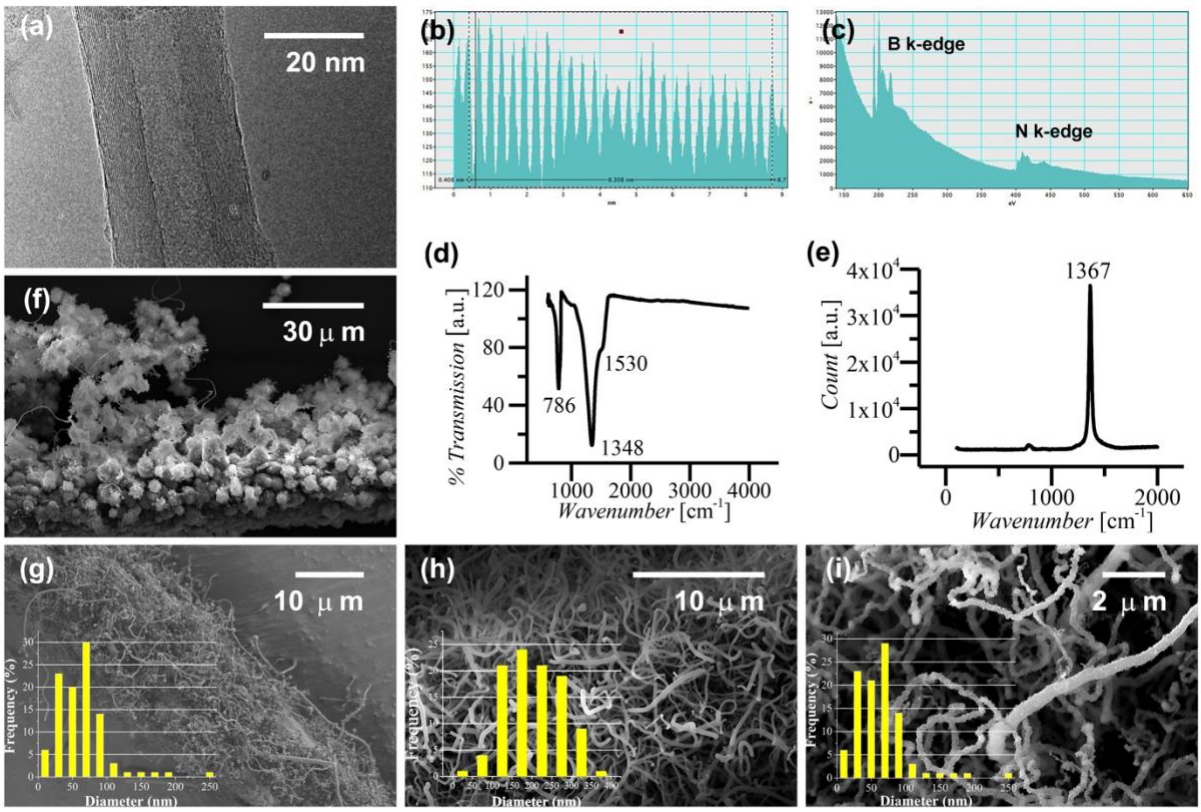

Figure 3. (a) HRTEM image of a single BNNT, (b) profile analysis of a single BNNT, (c) EELS of the as-synthesized BNNTs, (d) FTIR spectra of as-synthesized BNNTs, (e) RAMAN spectrum of BNNTs, (f) SEM image of SiC_f without any surface decoration. SEM images of different BNNTs growth periods: (g) 30 minutes, (h) 60 minutes, (i) 90 minutes.

The morphologies of BNNTs were also evaluated with various growth times of 30, 60, and 90 minutes with respect to nanotube density and surface coverage. Presented in **Error! Reference source not found.**(g), 30 minute growth time resulted in low yield and partial coverage of the SiC_f surface, which is highly undesirable for surface interactions. As clearly shown in **Error! Reference source not found.**(h), the 60 minute growth time resulted in the best outcome, a highly covered surface, and bamboo-like tube morphology. On the other hand, at the 90 minute growth time, BNNTs resulted in deformed BNNT tube morphology compared to bamboo-like tubes present in the 60 minutes growth time evident in a closer view SEM images (**Error! Reference source not found.**(i)). A curvy and curly bamboo-like morphology, high-yield, homogeneous diameter distribution, and full coverage of

BNNTs achieved with the 60 minutes of growth time may offer higher IFSS values. Additionally, fuzzy BNNT architectures at preform stages can increase the ILSS of composites by fiber-fiber interaction through the "hook and loop" mechanism when intertwined BNNTs were considered.

3.2. Mechanical Test Results

3.2.1. Single Fiber Tensile Test

Tensile test results for as-received, desized, and BNNTs/SiC_f were summarized in Table 1**.** Since BNNTs growth in the GVT-BOCVD system is a high-temperature process, the SiC_f was exposed to various gases at temperatures between 1000 °C and 1200 °C and studied to explore the effect of reactant and temperature concerning the overall mechanical properties of these fibers. The average tensile strength of desized SiC_f (with DMF) was similar to as-received SiC_f, with 2295 ± 36 MPa for desized compared to 2101 ± 98 MPa for the as-received SiC_f, which was in line with reported values by the supplier [42]. To identify the most significant strength loss due to BNNT growth by GVT-BOCVD system, a heat treatment at 1200 °C, the highest recognized temperature during a growth process, was studied, and the strength of SiC_f decreased to 1833 ± 87 MPa. This strength loss was observed to be more severe under an ammonia atmosphere, with the tensile strength of the SiC_f dropping to 1088 ± 59 MPa. However, the fuzzy BNNTs/SiC_f (sample code T-5 in Table 1) showed no further strength loss (926 ± 46 MPa) than T-4. Furthermore, studies on the literature where BN coating was applied to the surface of the SiC fibers also show a similar decrease in the tensile strength of the fibers, further supporting the non-effect of the BNNT growth on the fiber surface [43, 44]. Moreover, BNNT/SiC_f showed a high Weibull modulus indicating a uniform distribution of flaws along with the fiber and little variation in the tensile strength (**Error! Reference source not found.**(b)). All sample codes were given in detail in Table 1.

Table 1. Sample codes and conditions during BNNT growth onto SiC_f for evaluation of tensile strength.

Sample Code	Number of Tested Specimen	Conditions	Tensile Strength [MPa]	Weibull Modulus
T-1	44	As-received SiC_f	2101 ± 98	3.31
T-2	43	Desized (with DMF)	2295 ± 36	3.51
T-3	13	Desized /heat-treated at 1200 °C	1833 ± 87	3.30
T-4	35	Desized/ catalyzed/ NH_3 flow, 1200 °C	1088 ± 59	3.31
T-5	34	BNNT on SiC_f as 'fuzzy fiber'	926 ± 46	4.01

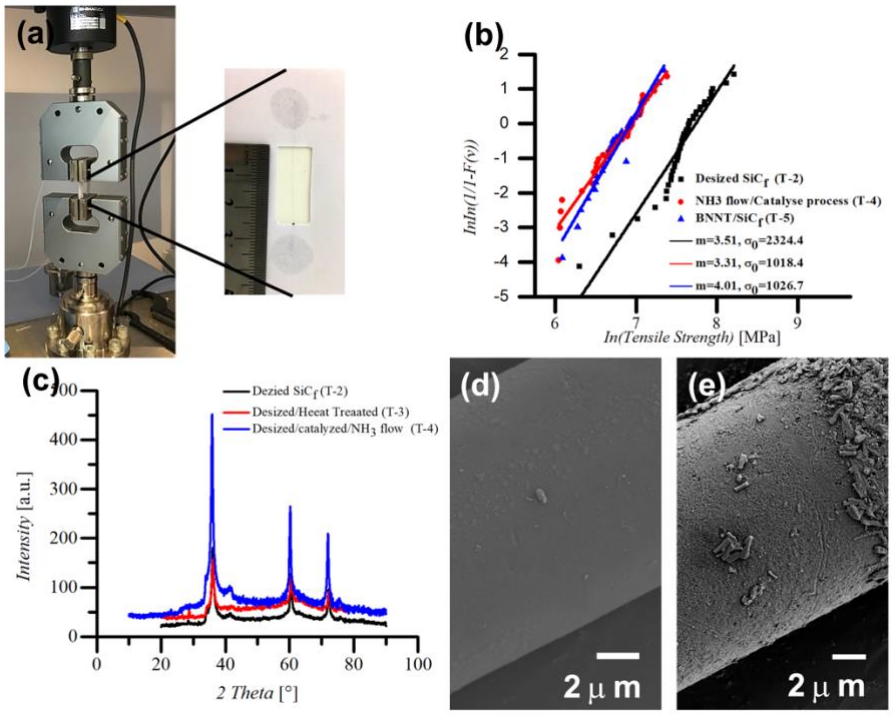

Figure 4. (a) Tensile test setup and prepared specimen, (b) tensile test results of T-2, T-4, T-5, and BNNTs/SiC_f, (c) XRD spectrum of T-2, T-3, T-4 samples. SEM images of (d) T-3 and (e) T-4.

XRD analysis was performed to determine this significant decrease wherein typical SiC_f peaks of the β-SiC phase were observed for desized, heat-treated, and NH_3 flown catalyzed fibers to identify the effect of NH_3 reactant gas on the SiC_f. The peaks at 36.15°, 60.2^O and 71.8^O of 2Θ values corresponded to (111), (220), and (311) planes, respectively, which are typical for a SiC_f (**Error! Reference source not found.**(c)). 2θ of 41.5^O in the XRD

spectrum denoted the disordered stacking structure of the β-SiC ((200) plane). Although SEM images of the neat SiC_f (**Error! Reference source not found.**(d)) which were heat-treated at 1200 °C (T-3), depicted a smooth fiber surface with no degradation or roughness. Significant β-SiC crystal growth was detected by calculating the crystallite size of the β-SiC ((111) plane) via a Scherer equation from XRD data. While the crystallite size of the β-SiC in desized SiC_f (T-2) was 3.29 nm, after heat treatment at 1200 °C (T-3), the crystallite size of the β-SiC was 10.91 nm. In addition, for fibers exposed to BNNT growth conditions (T-4), the crystallite size of the β-SiC was 23.38 nm, and these crystals can be seen in **Error! Reference source not found.**(e). It was also reported that the SiC materials exhibited crystal growth at high temperatures, and this growth was related to excess carbon content[45] Hi Nicalon type is the SiC_f which has the most excess carbons, and these carbons were able to inhibit the crystal growth. In this case, with the aid of the inhibitive effect of the excess carbons, fiber degradation was not observed in the SEM images of the fibers despite crystal growth[45].

We have experienced significant mechanical strength loss after modifying the SiC fibers when exposed to high temperatures and an ammonia atmosphere. Similar results related to the decreased thermo-mechanical stability of SiC_f at elevated temperatures were reported in the literature. [45-48] Mah, *et al.*[46] investigated the tensile strength of SiC_f under different temperatures and atmospheres, presenting a decrease in tensile strength from 1230 MPa to 848 MPa when the temperature was increased to 1400 °C under Ar flow. Furthermore, when they introduced oxygen to a high-temperature environment, they reported a more significant strength regression (660 MPa), lower than the SiC fibers' tensile strength when exposed to an ammonia atmosphere. Since high temperature and air atmosphere are the commonly experienced conditions for SiC fibers in applications, our BNNT decoration causes no further degradation of SiC fibers other than what they would have been lost during its use in an application. SiC grain growth due to carbon monoxide (CO) evaporation at high

temperatures was also the main reason for the loss in mechanical performance.[48] Thus, measured tensile strength for the fibers after BNNTs growth is in accord with the reported values in strength loss attributed to crystal growth during exposure to elevated temperatures.

3.2.2. Microbonding Test

A microbond test was performed to investigate the effect of the BNNTs on the interfacial interactions of F/M. Several methods, such as the nano-indentation method [49], single fiber fragmentation test, and microbond tests [50] have been reported for investigating the IFSS of F/M systems quantitatively. Required expensive equipment and complex specimen preparation of nano-indentation, and the inappropriateness of the single fiber fragmentation test for brittle samples, a microbond test system was chosen to overcome these limitations. The microbond test has been utilized for polymeric [51], glass [52] and carbonaceous single fibers [53, 54] *etc.* due to the simple sample preparation and testing equipment, as well as its low cost, and referred to as an effective tool to study the mechanical behavior of the fiber-matrix interfaces in earlier studies [55, 56]. Photos and schematics of the customized microbond test setup equipped to the UTM can be seen in **Error! Reference source not found.Error! Reference source not found.** (a-b)**,** respectively. The most important test parameters of the distance between the blades and the embedded fiber length (microdroplet length) are denoted by $\underline{w}$ and $\underline{L}$, respectively. To the best of our knowledge, this kind of module design is unique for such a fuzzy architecture study, and we hope to encourage similar tests to be used with similar approaches, through a straightforward deployability characteristic of most UTM equipment.

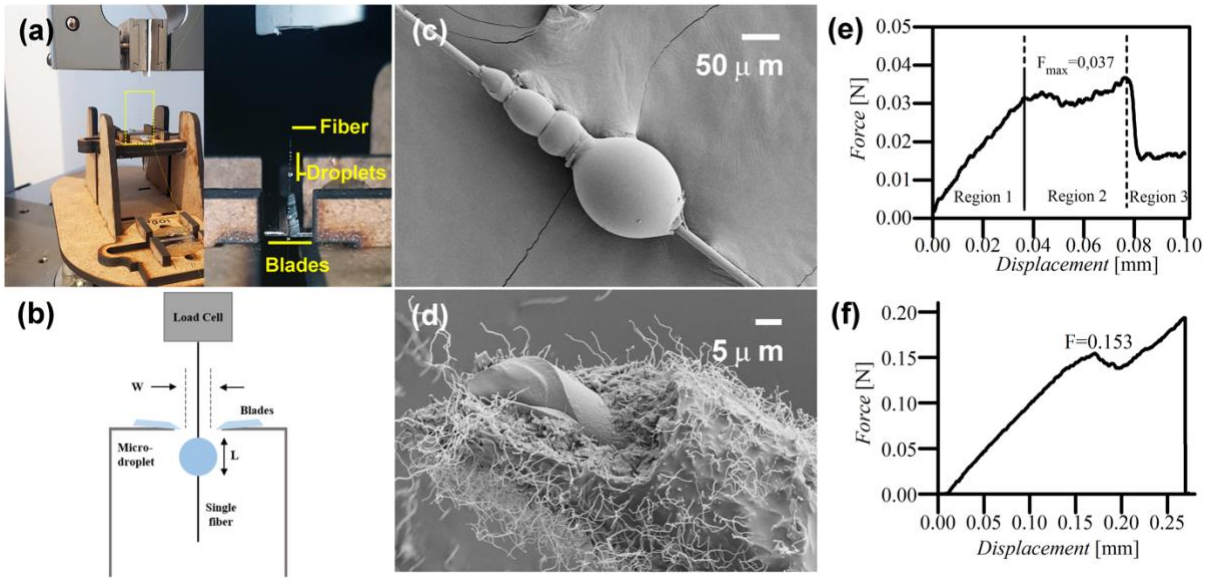

Figure 4. SiC_f and BNNTs/SiC_f IFSS test results and characterizations (a) Photo and (b) schematic view of the home built microdroplet test setup, (c) SEM image of fiber with the epoxy droplet, (d) BNNT coated SiC_f sample after microbond test. Load – displacement curves of (e) as-received SiC_f and (f) BNNTs/SiC_f.

During the microbond test, if fiber rupture was observed, the data was deemed unusable. After testing various specimens, the number of successful tests was strongly dependent on the embedded length with epoxy [57]. To obtain an interval of optimum embedded length, samples with 100 - 600 μm embedded length were tested, and it was found that the ones with 150 – 250 μm embedded length showed the highest number of successful tests. Different interfacial shear mechanisms, such as shear debonding, microdroplet slippage, and sequential two droplets debonding [58, 59] were also observed, as also indicated in the representative SEM image showing the droplets created on the SiC fiber (**Error! Reference source not found.**(**Error! Reference source not found.**c)) and in the representative curve (**Error! Reference source not found.**(**Error! Reference source not found.**e)). In region I, debonding of F/M interface started and was propagated until the peak force used in IFSS calculations; then droplet slippage occurred in region II with an insignificant increase in

force. After full debonding, droplets started to move along the fiber axis with small resistance of frictional force, as presented in Region 3.

BNNTs/SiC_f were tested with a similar test setup to the one used for the as-received SiC_f to investigate the effect of BNNTs on the failure mode and IFSS of the F/M system. Initial tests on BNNTs/SiC_f droplets showed no resistance to slippage, indicating poor interfacial interactions between epoxy droplets and BNNTs due to the poor wettability of BNNTs, where similar findings were also reported by Zhu *et al.* [22]. In which, SiC_f/SiC composites were fabricated with BNNTs as interphase material, and the mechanical properties of the composite were investigated with and without BNNTs. They observed that hybrid BNNT composites exhibited inferior mechanical properties in terms of flexural strength than those without BNNTs, which was attributed to the high amount of porosity and voids in the interface due to the poor wettability of BNNTs. Hence, to overcome the poor wettability characteristics of BNNTs on SiC_f, plasma treatment was applied for two minutes by exposing BNNTs/SiC_f fibers to oxygen plasma at room temperature before the epoxy microdroplet formation and referred to as 2m-BNNTs/SiC_f. Such a process is expected to weaken the highly apolar nature of the BNNT surface by introducing new defects, leading to better wettability. To the best of our knowledge, such post-treatment has not been so far reported for BNNTs for the modification of a fuzzy fiber surface. During the IFSS tests on 2m-BNNTs/SiC_f, no slippage was observed, and fibers were broken, indicating the expected strong interface thus, no meaningful data could be collected. To overcome this problem, exposure time to plasma onto BNNT/SiC_f was decreased from two minutes to one minute and referred to 1m-BNNTs/SiC_f.

Since the interface in composites should be neither excessively strong nor weak, an optimum interface strength needs to be attained. The good adhesion of the epoxy matrix due to the before-mentioned oxygen plasma treatment can be seen in the fracture surface SEM image of the fiber (**Error! Reference source not found.**(d)). Accordingly, weak F/M bonding is

preferable for brittle materials since weak bonding allows extra energy dissipation mechanisms such as fiber pullout, debonding, and fiber bridging, increasing the material's toughness [60]. The tests on the 1m- BNNTs/SiC_f consequently yielded successful tests. During the tests, the load increased until the microdroplet started to fail. Subsequently, a load drop was observed due to the failure of the matrix, and then the load was increased again until the fiber rupture. At the time of the second load increase, the droplet fracture was hindered, and the load was carried by the fiber. The first load drop point was attained as the debonding force (Figure 5(f)). Sato *et al.* [61] speculate that when the IFSS of the interface is too high, the interface can not be entirely debonded before matrix failure, which is observed in this study (Figure 5(d)) as well. Thus, we have selected to use F_{max} before the first force drop as the pullout force. Although this approach results in lower IFFS value calculations, in practice, these IFFS values are the highest attainable IFFS values with epoxy matrix. This problem was not present in the micro droplet testing of the neat SiC fibers, as shown in the supporting information.

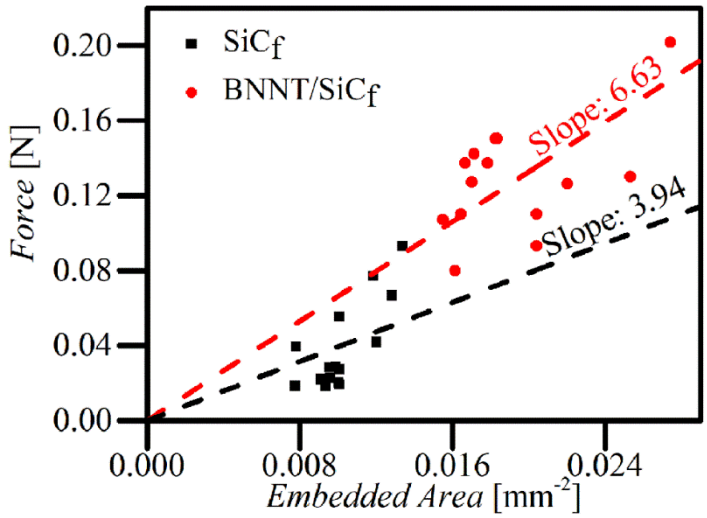

Figure 5. Force vs. Embedded area plot for the neat SiC_f and BNNT/SiC_f.

Through the successful 15 tests from baseline specimens and 14 tests from BNNTs/SiC_fs, the force–embedded area plot was examined for IFSS evaluation. IFSS can be determined by simply averaging the calculated data or the linear regression slope of the force–embedded

area plot that intercepts origin [57]. By averaging, IFSS of neat SiC_f and BNNTs/SiC_f were determined as 3.61 ± 0.43 MPa and 6.78 ± 0.35 MPa with an 87.8% improvement, respectively (Table 2). The data plots for the microbond tests were given in **Error! Reference source not found.**. The slopes of the regression lines were 3.94 and 6.63 for baselines and BNNT/SiC_fs, which can also represent the IFSS in MPa and shows a 68.3% enhancement. It was clearly seen that the fuzzy architecture of BNNT/SiC_f improved the interfacial interactions of the SiC_f/matrix. This effect was theorized to be the result of the "Velcro-like" entanglement of the tubes as described in the article by Hart *et al.* [8] in which they discuss the surface-anchored nanotubes hooking into the nanotubes on the matrix fibers, creating "Velcro-like" connections to prevent fiber-fiber sliding and enhancing the interlaminar strength of the composite. In their work, they describe hook and loop mechanisms occurring in two different settings. First, fiber BNNTs interact with the matrix BNNTs on the SiC fiber and second, securely embedded fiber BNNTs inside the matrix act as a "hook" to matrix "loop". Our IFFS test can only evaluate the second mechanism described as BNNTs embedded in the epoxy matrix acts as "hooks" for the matrix "loops". The scattering in the data for both types of specimens can be attributed to the variations of the test parameters such as the different surface texture of the fibers with or without BNNT deployment, size, and geometry of the microdroplets, and contact point of microdroplet and the blades [57, 62].

Table 2. Calculated IFFS values for the BNNTs/SiC_f samples.

Sample	Sample Properties	IFSS [Nmm^{-2}]
As-SiC_f	As-received SiC_f	3.61 ± 0.43
1m-BNNT/SiC_f	1 min plasma etched BNNT/SiC_f	6.78 ± 0.35

Based on our knowledge, there is no reported study investigating the IFSS of the single SiC fibers by the microbond test method. Chai *et al.* performed the IFSS test for the single SiC

fibers by the nano-indentation method and reported the IFSS result as around 75 MPa.[49] However, this method and microdroplet are not comparable in the case of IFSS results because of the implementation of the test and different matrix types as they used a nano-indenter to push the SiC fiber out of the ceramic matrix. Also, Qian *et al.* [63] reported the IFSS of CNT-grown carbon fibers and epoxy matrix by pullout and indentation method. While they observed a 57% increase in IFSS by CNT growth through indentation tests, the IFSS was unchanged in pullout tests which shows the strong influence of the measurement technique on the IFSS values. Another study by Harwell *et al.* [64] investigated the bond strength of SiC coated ribbon carbon fibers and epoxy matrix, which is a similar interface to this study. Analogously to this work, force values scattered in a low range of 0.15 to 0.40 N, and the IFSS of the SiC_f/epoxy interface reported as up to 12.2 MPa. Moreover, a significant amount of fiber rupture was also observed. The microbond test to determine IFSS depends on those parameters heavily. Thus, the variety of parameters (such as embedded length, coating thickness, and microbond test nature) involved in the microbond test causes a diversity of IFSS values. Different IFSS values were reported for the same materials when various parametric studies were performed [52, 65-68]**,** such as reported for glass fibers [52, 68] and carbon fibers [66, 67] by using microdroplet tests. Accordingly, all parameters involved in the measurement should be considered comprehensively while comparing results interlaboratory.

4. Conclusion

F/M interface interactions of SiC_f and matrix material can be enhanced by growing "fuzzy fiber" BNNTs on the surface of such fibers via simple catalyst decoration followed by the GVT-BOCVD method at a relatively low temperature as 1200 °C, compared to earlier studies in the literature. As-grown BNNTs show full coverage of the SiC_f surface, with a bamboo-like morphology and a 20 to 150 nm tube diameter. It was found that BNNT fuzzy fiber caused no further damage to heat-treated SiC_f, and fibers preserved their structural integrity. A

microdroplet test showed that “fuzzy fiber” architecture in the BNNTs/SiC_f increased the IFSS by at least 87.8%, only limited by the strength of the epoxy matrix. It is suggested that this “fuzzy fiber” coating enhances the interfacial interactions with two mechanisms: (1) Increased fiber surface area, (2) interlocking of the BNNTs in a “Velcro-like” fashion. Although the IFSS data reported in this research has been gathered from the epoxy/SiC fiber interface, which does not directly represent the CMC interfaces, it provides significant insight into the F/M interface between the SiC fibers and the matrix. The improved IFSS values of single SiC fibers were able to be collected quickly and easily from the epoxy droplet system, providing an effective evaluation tool before moving to CMCs Further work will evaluate the effectiveness of the BNNT layer the CMC materials using ceramic materials as matrix and SiC fibers. For advanced applications such as those demanded in the aerospace industry, enhanced fiber-matrix interaction for ceramic matrix composites can be achieved by engineering such hierarchical architectures on SiC fibers.

Acknowledgments

The authors would like to acknowledge the Safran Herakles company for funding this project. The authors would like to thank the National Research Center on Membrane Technologies and ITU universal Textile Design Center for their support. The authors would also like to thank Melike Mercan Yıldızhan and Deniz Ürk for their help in this research. Authors Deniz Köken and Ayşemin Top contributed equally to this work.

Supporting Information

Supporting Informııation is supplied separately

References

1. J. Nasser, K. Steinke, H.-S. Hwang, H. Sodano, Nanostructured ZnO Interphase for Carbon Fiber Reinforced Composites with Strain Rate Tailored Interfacial Strength, Adv. Mater. Interfaces, 7 (2020) 1901544. https://doi.org/10.1002/admi.201901544

2. M.H. Malakooti, Z. Zhou, J.H. Spears, T.J. Shankwitz, H.A. Sodano, Biomimetic nanostructured interfaces for hierarchical composites, Adv. Mater. Interfaces, 3 (2016) 1500404. https://doi.org/10.1002/admi.201500404
3. D. Ding, W. Zhou, F. Luo, M. Chen, D. Zhu, Dip-coating of boron nitride interphase and its effects on mechanical properties of SiCf/SiC composites, Mater. Sci. Eng., A, 543 (2012) 1-5.https://doi.org/10.1016/j.msea.2012.01.118
4. N.I. Baklanova, O.I. Kiselyova, A.T. Titov, T.M. Zima, Microstructural features of the ZrO2 interfacial coatings on SiC fibers before and after exposition to air at high temperatures, J. Eur. Ceram. Soc., 28 (2008) 1687-1696.https://doi.org/10.1016/j.jeurceramsoc.2007.11.008
5. Y. Zheng, S. Wang, Synthesis of boron nitride coatings on quartz fibers: Thickness control and mechanism research, Appl. Surf. Sci., DOI https://doi.org/10.1016/j.apsusc.2011.07.092(2011).https://doi.org/10.1016/j.apsusc.2011.07.092
6. B.J.T. Lu Shen, William S. Willis, Francis S. Galasso, Steven L. Suib, Characterization of Dip-Coated Boron Nitride on Silicon Carbide Fibers, J. Am. Ceram. Soc., 77 (1994) 1011-1016. https://doi.org/10.1111/j.1151-2916.1994.tb07260.x
7. E.J. Garcia, B.L. Wardle, A. John Hart, N. Yamamoto, Fabrication and multifunctional properties of a hybrid laminate with aligned carbon nanotubes grown In Situ, Compos. Sci. Technol., 68 (2008) 2034-2041.https://doi.org/10.1016/j.compscitech.2008.02.028
8. A.H.C. Hart, R. Koizumi, J. Hamel, P.S. Owuor, Y. Ito, S. Ozden, S. Bhowmick, S.A. Syed Amanulla, T. Tsafack, K. Keyshar, R. Mital, J. Hurst, R. Vajtai, C.S. Tiwary, P.M. Ajayan, Velcro-Inspired SiC Fuzzy Fibers for Aerospace Applications, ACS Appl. Mater. Interfaces, 9 (2017) 13742-13750.https://doi.org/10.1021/acsami.7b01378
9. S.S. Wicks, R.G. de Villoria, B.L. Wardle, Interlaminar and intralaminar reinforcement of composite laminates with aligned carbon nanotubes, Compos. Sci. Technol., 70 (2010) 20-28.https://doi.org/10.1016/j.compscitech.2009.09.001
10. K. Sun, J. Yu, C. Zhang, X. Zhou, In situ growth carbon nanotube reinforced SiCf/SiC composite, Mater. Lett., 66 (2012) 92-95.https://doi.org/10.1016/j.matlet.2011.07.105
11. K. König, S. Novak, A. Ivekovič, K. Rade, D. Meng, A.R. Boccaccini, S. Kobe, Fabrication of CNT-SiC/SiC composites by electrophoretic deposition, J. Eur. Ceram. Soc., 30 (2010) 1131-1137.https://doi.org/10.1016/j.jeurceramsoc.2009.07.027
12. S. Zhao, X. Zhou, J. Yu, P. Mummery, SiC/SiC composite fabricated with carbon nanotube interface layer and a novel precursor LPVCS, Fusion Eng. Des., 89 (2014) 131-136.https://doi.org/10.1016/j.fusengdes.2014.01.051
13. R.B. Mathur, S. Chatterjee, B.P. Singh, Growth of carbon nanotubes on carbon fibre substrates to produce hybrid/phenolic composites with improved mechanical properties, Compos. Sci. Technol., 68 (2008) 1608-1615.https://doi.org/10.1016/j.compscitech.2008.02.020
14. J.L. Qiuhong Zhang, Ryan Sager, Liming Dai, Jeffery Baur, Hierarchical composites of carbon nanotubes on carbon fiber: Influence of growth condition on fiber tensile properties, Compos. Sci. Technol., 69 (2009) 594-601.https://doi.org/10.1016/j.compscitech.2008.12.002
15. X. Liu, L. Zhang, X. Yin, F. Ye, Y. Liu, L. Cheng, Flexible thin SiC fiber fabrics using carbon nanotube modification for improving electromagnetic shielding properties, Mater. Des., 104 (2016) 68-75.https://doi.org/10.1016/j.matdes.2016.05.005
16. W. Feng, L. Zhang, Y. Liu, X. Li, L. Cheng, B. Chen, Thermal and mechanical properties of SiC/SiC-CNTs composites fabricated by CVI combined with electrophoretic deposition, Mater. Sci. Eng., A, 626 (2015) 500-504.https://doi.org/10.1016/j.msea.2014.12.105
17. K. Hata, D.N. Futaba, K. Mizuno, T. Namai, M. Yumura, S. Iijima, Water-Assisted Highly Efficient Synthesis of Impurity-Free Single-Walled Carbon Nanotubes, Science, 306 (2004) 1362-1364.https://doi.org/10.1126/science.1104962

18. N.G. Chopra, R. Luyken, K. Cherrey, V.H. Crespi, M.L. Cohen, S.G. Louie, A. Zettl, Boron nitride nanotubes, Science, 269 (1995) 966-967.https://doi.org/10.1126/science.269.5226.966
19. D. Golberg, Y. Bando, Y. Huang, T. Terao, M. Mitome, C. Tang, C. Zhi, Boron nitride nanotubes and nanosheets, ACS nano, 4 (2010) 2979-2993.https://doi.org/10.1021/nn1006495
20. A. Rubio, J.L. Corkill, M.L. Cohen, Theory of graphitic boron nitride nanotubes, Phys. Rev. B: Condens. Matter, 49 (1994) 5081.https://doi.org/10.1103/PhysRevB.49.5081
21. J. Hurst, Boron Nitride Nanotubes Grown on Commercial Silicon Carbide Fiber Tow and Fabric, in: S. Mathur, S.S. Ray (Eds.) Nanostructured Materials and Nanotechnology Vl, The American Ceramic Society2013, pp. 21-29. https://doi.org/10.1002/9781118217511.ch3
22. G. Zhu, S. Dong, D. Ni, C. Xu, D. Wang, Microstructure, mechanical properties and oxidation resistance of SiCf/SiC composites incorporated with boron nitride nanotubes, RSC Adv., 6 (2016) 83482-83492.https://doi.org/10.1039/C6RA16496J
23. P. Nautiyal, C. Rudolf, A. Loganathan, C. Zhang, B. Boesl, A. Agarwal, Directionally Aligned Ultra‐Long Boron Nitride Nanotube Induced Strengthening of Aluminum‐Based Sandwich Composite, Adv. Eng. Mater., 18 (2016) 1747-1754. https://doi.org/10.1002/adem.201600212
24. F. Rebillat, J. Lamon, A. Guette, The concept of a strong interface applied to SiC/SiC composites with a BN interphase, Acta Mater., 48 (2000) 4609-4618.https://doi.org/10.1016/S1359-6454(00)00247-0
25. F. Rebillat, J. Lamon, R. Naslain, E. Lara‐Curzio, M.K. Ferber, T.M. Besmann, Properties of multilayered interphases in SiC/SiC chemical‐vapor‐infiltrated composites with “weak” and “strong” interfaces, J. Am. Ceram. Soc., 81 (1998) 2315-2326.https://doi.org/10.1111/j.1151-2916.1998.tb02627.x
26. S. Bertrand, R. Pailler, J. Lamon, Influence of strong fiber/coating interfaces on the mechanical behavior and lifetime of Hi‐Nicalon/(PyC/SiC) n/SiC minicomposites, J. Am. Ceram. Soc., 84 (2001) 787-794.https://doi.org/10.1111/j.1151-2916.2001.tb00742.x
27. S. Dong, Y. Katoh, A. Kohyama, Preparation of SiC/SiC composites by hot pressing, using Tyranno‐SA fiber as reinforcement, J. Am. Ceram. Soc., 86 (2003) 26-32.https://doi.org/10.1111/j.1151-2916.2003.tb03272.x
28. S. Pasquier, J. Lamon, R. Naslain, Tensile static fatigue of 2D SiC/SiC composites with multilayered (PyC–SiC)n interphases at high temperatures in oxidizing atmosphere, Composites Part A, 29 (1998) 1157-1164.https://doi.org/10.1016/S1359-835X(98)00093-1
29. C. Zhi, Y. Bando, C. Tan, D. Golberg, Effective precursor for high yield synthesis of pure BN nanotubes, Solid State Commun., 135 (2005) 67-70.https://doi.org/10.1016/j.ssc.2005.03.062
30. C.H. Lee, J. Wang, V.K. Kayatsha, J.Y. Huang, Y.K. Yap, Effective growth of boron nitride nanotubes by thermal chemical vapor deposition, Nanotechnology, 19 (2008) 455605.https://doi.org/10.1088/0957-4484/19/45/455605
31. A. International, D 3379 – 75 Standard Test Method for Tensile Strength and Young’s Modulus for High-Modulus Single-Filament Materials, 1989,
32. A. Khalili, K. Kromp, Statistical properties of Weibull estimators, J. Mater. Sci, 26 (1991) 6741-6752.https://doi.org/10.1007/BF00553701
33. Frank W. Zok, Xiuyen Chen, C.H. Weber, Tensile Strength of Sic Fibers, J. Am. Ceram. Soc., 78 (1995).https://doi.org/10.1111/j.1151-2916.1995.tb08919.x
34. Y. Liu, N. Chai, H. Qin, Z. Li, F. Ye, L. Cheng, Tensile fracture behavior and strength distribution of SiCf/SiC composites with different SiBN interface thicknesses, Ceram. Int., 41 (2015) 1609-1616.https://doi.org/10.1016/j.ceramint.2014.09.098
35. D. Köken, Synthesis and optimization of boron nitride nanotubes for stable aqueous dispersions, Faculty of Engineering and Natural Sciences, Sabancı University, 2016,

36. K. Yum, M.-F. Yu, Measurement of wetting properties of individual boron nitride nanotubes with the Wilhelmy method using a nanotube-based force sensor, Nano Lett., 6 (2006) 329-333.https://doi.org/10.1021/nl052084l
37. L. Li, X. Liu, X.J. Dai, L. Li, Y. Chen, Surface wetting processing on BNNT films by selective plasma modes, Chin. Sci. Bull., 58 (2013) 3403-3408.https://doi.org/10.1007/s11434-013-5859-2
38. D. Golberg, W. Han, Y. Bando, L. Bourgeois, K. Kurashima, T. Sato, Fine structure of boron nitride nanotubes produced from carbon nanotubes by a substitution reaction, J. Appl. Phys., 86 (1999) 2364-2366.https://doi.org/10.1063/1.371058
39. D. Golberg, Y. Bando, L. Bourgeois, K. Kurashima, T. Sato, Insights into the structure of BN nanotubes, Appl. Phys. Lett., 77 (2000) 1979-1981.https://doi.org/10.1063/1.1313251
40. P. Amir, Z. Chunyi, B. Yoshio, N. Tomonobu, G. Dmitri, A comprehensive analysis of the CVD growth of boron nitride nanotubes, Nanotechnology, 23 (2012) 215601.https://doi.org/10.1088/0957-4484/23/21/215601
41. L. Wirtz, A. Rubio, R.A. de La Concha, A. Loiseau, Ab initio calculations of the lattice dynamics of boron nitride nanotubes, Phys. Rev. B: Condens. Matter, 68 (2003) 045425.http://dx.doi.org/10.1103/PhysRevB.68.045425
42. E. Buet, C. Sauder, S. Poissonnet, P. Brender, R. Gadiou, C. Vix-Guterl, Influence of chemical and physical properties of the last generation of silicon carbide fibres on the mechanical behaviour of SiC/SiC composite, J. Eur. Ceram. Soc., 32 (2012) 547-557.https://doi.org/10.1016/j.jeurceramsoc.2011.09.023
43. M. Yuan, T. Zhou, J. He, L. Chen, Formation of boron nitride coatings on silicon carbide fibers using trimethylborate vapor, Appl. Surf. Sci., 382 (2016) 27-33.https://doi.org/10.1016/j.apsusc.2016.04.080
44. S. Guo, Y. Kagawa, Temperature dependence of tensile strength for a woven Boron‐Nitride‐Coated Hi‐Nicalon™ SiC fiber‐reinforced silicon‐carbide‐matrix composite, J. Am. Ceram. Soc., 84 (2001) 2079-2085.https://doi.org/10.1111/j.1151-2916.2001.tb00961.x
45. M. Takeda, J.-i. Sakamoto, Y. Imai, H. Ichikawa, Thermal stability of the low-oxygen-content silicon carbide fiber, Hi-Nicalon, Compos. Sci. Technol., 59 (1999) 813-819.https://doi.org/10.1016/S0266-3538(99)00012-3
46. N.L.H. T. Mah, D. E. McCullum, J. R. Hoenigman, H. M. Kim, A. P. Katz, H. A. Lipsitt, Thermal stability of SiC fibres (Nicalon), J. Mater. Sci, DOI https://doi.org/10.1007/BF01120029(1984) 1191-1201.https://doi.org/10.1007/BF01120029
47. M.W. Narayanan Janakiraman, Jörg Schuhmacher, Klaus Müller, Joachim Bill, Fritz Aldinger, Thermal Stability, Phase Evolution, and Crystallization in Si-B-C-N Ceramics Derived from a Polyborosilazane Precursor, J. Am. Ceram. Soc., 7 (2002) 1807-1814.https://doi.org/10.1111/j.1151-2916.2002.tb00357.x
48. S. Cao, J. Wang, H. Wang, Formation mechanism of large SiC grains on SiC fiber surfaces during heat treatment, CrystEngComm, 18 (2016) 3674-3682.https://doi.org/10.1039/C6CE00427J
49. Y. Chai, H. Zhang, X. Zhou, Y. Zhang, Effects of silicon ion irradiation on the interface properties of SiC f /SiC composites, Ceram. Int., 44 (2018) 2165-2169.https://doi.org/10.1016/j.ceramint.2017.10.169
50. J. Karger-Kocsis, H. Mahmood, A. Pegoretti, Recent advances in fiber/matrix interphase engineering for polymer composites, Prog. Mater Sci., 73 (2015) 1-43.https://doi.org/10.1016/j.pmatsci.2015.02.003
51. M. Mohammadalipour, M. Masoomi, M. Ahmadi, S. Safi, Interfacial shear strength characterization of GMA-grafted UHMWPE fiber/epoxy/nano clay hybrid nanocomposite materials, RSC Adv., 6 (2016) 41793-41799.https://doi.org/10.1039/C6RA05027A
52. B. Dastorian Jamnani, S. Hosseini, S. Rahmanian, S. Abdul Rashid, S. Keshan Balavandy, Grafting carbon nanotubes on glass fiber by dip coating technique to enhance

tensile and interfacial shear strength, J. Nanomater, 2015 (2015).https://doi.org/10.1155/2015/149736
53. X. Zhang, X. Fan, C. Yan, H. Li, Y. Zhu, X. Li, L. Yu, Interfacial microstructure and properties of carbon fiber composites modified with graphene oxide, ACS Appl. Mater. Interfaces, 4 (2012) 1543-1552.https://doi.org/10.1021/am201757v
54. X.Z. Tang, B. Yu, R.V. Hansen, X. Chen, X. Hu, J. Yang, Grafting low contents of branched polyethylenimine onto carbon fibers to effectively improve their interfacial shear strength with an epoxy matrix, Adv. Mater. Interfaces, 2 (2015) 1500122.https://doi.org/10.1002/admi.201500122
55. Z. Dai, F. Shi, B. Zhang, M. Li, Z. Zhang, Effect of sizing on carbon fiber surface properties and fibers/epoxy interfacial adhesion, Appl. Surf. Sci., 257 (2011) 6980-6985.https://doi.org/10.1016/j.apsusc.2011.03.047
56. C. Wang, Y. Li, L. Tong, Q. Song, K. Li, J. Li, Q. Peng, X. He, R. Wang, W. Jiao, The role of grafting force and surface wettability in interfacial enhancement of carbon nanotube/carbon fiber hierarchical composites, Carbon, 69 (2014) 239-246.https://doi.org/10.1016/j.carbon.2013.12.020
57. J. Craven, R. Cripps, C. Viney, Evaluating the silk/epoxy interface by means of the microbond test, Composites Part A, 31 (2000) 653-660.https://doi.org/10.1016/S1359-835X(00)00042-7
58. B. Miller, P. Muri, L. Rebendfeld, A microbond Method for Determination of the Shear Strength of a Fiber/Resin Interface, Compos. Sci. Technol., 28 (1987) 18-32.https://doi.org/10.1016/0266-3538(87)90059-5
59. B.M. Umesh Gaur, Microbond Method for Determination of the Shear Strength of a Fiber/Resin İnterface: Evaluation of Experimental Parameters, Compos. Sci. Technol., 34 (1989) 35-51.https://doi.org/10.1016/0266-3538(89)90076-6
60. Z.X.a.L. Li, Understanding Interfaces and Mechanical Properties of Ceramic Matrix Composites, in: I.M. Low (Ed.) Advances in Ceramic Matrix Composites, Woodhead Publishing Limited2014.https://doi.org/10.1533/9780857098825.2.267
61. M. Sato, E. Imai, J. Koyanagi, Y. Ishida, T. Ogasawara, Evaluation of the interfacial strength of carbon-fiber-reinforced temperature-resistant polymer composites by the micro-droplet test, Adv. Compos. Mater, 26 (2017) 465-476.https://doi.org/10.1080/09243046.2017.1284638
62. M. Zu, Q. Li, Y. Zhu, M. Dey, G. Wang, W. Lu, J.M. Deitzel, J.W. Gillespie Jr, J.-H. Byun, T.-W. Chou, The effective interfacial shear strength of carbon nanotube fibers in an epoxy matrix characterized by a microdroplet test, Carbon, 50 (2012) 1271-1279.https://doi.org/10.1016/j.carbon.2011.10.047
63. H. Qian, A. Bismarck, E.S. Greenhalgh, G. Kalinka, M.S. Shaffer, Hierarchical composites reinforced with carbon nanotube grafted fibers: the potential assessed at the single fiber level, Chem. Mater., 20 (2008) 1862-1869.https://doi.org/10.1021/cm702782j
64. M. Harwell, D. Hirt, D. Edie, N. Popovska, G. Emig, Investigation of bond strength and failure mode between SiC-coated mesophase ribbon fiber and an epoxy matrix, Carbon, 38 (2000) 1111-1121.https://doi.org/10.1016/S0008-6223(99)00240-7
65. M. Pitkethly, J. Favre, U. Gaur, J. Jakubowski, S. Mudrich, D. Caldwell, L. Drzal, M. Nardin, H. Wagner, L. Di Landro, A round-robin programme on interfacial test methods, Compos. Sci. Technol., 48 (1993) 205-214.https://doi.org/10.1016/0266-3538(93)90138-7
66. S.-K. Kang, D.-B. Lee, N.-S. Choi, Fiber/epoxy interfacial shear strength measured by the microdroplet test, Compos. Sci. Technol., 69 (2009) 245-251.https://doi.org/10.1016/j.compscitech.2008.10.016
67. H. Wang, H. Wang, W. Li, D. Ren, Y. Yu, An improved microbond test method for determination of the interfacial shear strength between carbon fibers and epoxy resin, Polym. Test., 32 (2013) 1460-1465.https://doi.org/10.1016/j.polymertesting.2013.09.017

68. A. Godara, L. Gorbatikh, G. Kalinka, A. Warrier, O. Rochez, L. Mezzo, F. Luizi, A.W. Van Vuure, S.V. Lomov, I. Verpoest, Interfacial shear strength of a glass fiber/epoxy bonding in composites modified with carbon nanotubes, Compos. Sci. Technol., 70 (2010) 1346-1352.https://doi.org/10.1016/j.compscitech.2010.04.010